LETTER

doi:10.1038/nature14130

Recognition determinants of broadly neutralizing human antibodies against dengue viruses

Alexander Rouvinski[1,2]*, Pablo Guardado-Calvo[1,2]*, Giovanna Barba-Spaeth[1,2]*, Stéphane Duquerroy[1,2,3], Marie-Christine Vaney[1,2], Carlos M. Kikuti[1,2]†, M. Erika Navarro Sanchez[1,2]†, Wanwisa Dejnirattisai[4], Wiyada Wongwiwat[4], Ahmed Haouz[5], Christine Girard-Blanc[5], Stéphane Petres[5], William E. Shepard[6], Philippe Desprès[7]†, Fernando Arenzana-Seisdedos[8], Philippe Dussart[9]†, Juthathip Mongkolsapaya[4,10], Gavin R. Screaton[4] & Félix A. Rey[1,2,5]

Dengue disease is caused by four different flavivirus[1] serotypes, which infect 390 million people yearly with 25% symptomatic cases[2] and for which no licensed vaccine is available. Recent phase III vaccine trials showed partial protection, and in particular no protection for dengue virus serotype 2 (refs 3, 4). Structural studies so far have characterized only epitopes recognized by serotype-specific human antibodies[5,6]. We recently isolated human antibodies potently neutralizing all four dengue virus serotypes[7]. Here we describe the X-ray structures of four of these broadly neutralizing antibodies in complex with the envelope glycoprotein E from dengue virus serotype 2, revealing that the recognition determinants are at a serotype-invariant site at the E-dimer interface, including the exposed main chain of the E fusion loop[8] and the two conserved glycan chains. This 'E-dimer-dependent epitope' is also the binding site for the viral glycoprotein prM during virus maturation in the secretory pathway of the infected cell[9], explaining its conservation across serotypes and highlighting an Achilles' heel of the virus with respect to antibody neutralization. These findings will be instrumental for devising novel immunogens to protect simultaneously against all four serotypes of dengue virus.

Exposed at the surface of infectious mature dengue virus (DENV) particles, protein E is the sole target of neutralizing antibodies. It displays an icosahedral arrangement in which 90 E dimers completely coat the viral surface[10,11] and which is sensitive to the environmental pH. Upon entry of DENV into cells via receptor-mediated endocytosis, the acidic endosomal environment triggers an irreversible fusogenic conformational change in protein E that leads to fusion of viral and endosomal membranes[1]. A large fragment of E (termed sE for 'soluble E') lacking the C-terminal transmembrane anchor and a segment immediately preceding it (termed 'stem'), crystallizes as a dimer mimicking the organization of protein E on virions. The structure of the sE dimer has been determined by X-ray crystallography[8,12]. Protein E is relatively conserved, displaying about 65% amino-acid sequence identity when comparing the most distant DENV serotypes. In particular, there are two conserved N-linked glycosylation sites at positions N67 and N153. To examine its interaction with the antibodies, we selected four highly potent broadly neutralizing antibodies (bnAbs) identified in the accompanying work: 747(4) A11 and 747 B7 ('E-dimer-dependent epitope 2' (EDE2) group, requiring glycosylation at position N153 for efficient binding) and 752-2 C8 and 753(3) C10 (EDE1 group, binding regardless of the glycosylation at N153)[7]—referred to as A11, B7, C8 and C10 from hereon. The EDE2 bnAbs were isolated from the same patient (who had a secondary infection with serotype 2 (DENV-2)), and are somatic variants of the same immunoglobulin-G (IgG) clone, derived from the *IGHV3-74* and *IGLV2-23* germ lines. The heavy chain has a very long (26 amino acids, international ImMunoGeneTics information system (IMGT) convention) complementarity-determining region 3 (CDR H3). The EDE1 bnAbs were isolated from different patients and derive from VH and VL genes *IGHV3-64* and *IGKV3-11* (EDE1 C8, the patient appeared to have a primary infection of undetermined serotype) and *IGHV1-3* and *IGLV2-14* (EDE1 C10, from a patient with secondary DENV-1 infection). The analysis of the genes coding for these antibodies is summarized in Table 1.

Although it crystallizes as dimer[8,12,13], recombinant sE is mainly monomeric in solution. Interaction with the Fab or single-chain Fv (scFv) of the four bnAbs shifted the equilibrium to dimer. The crystal structures of the antibody/antigen complexes were determined as described in the Methods section, to a resolution between 3.0 and 3.2 Å for the complexes with B7, C10 and C8; and 3.85 Å for the complex with A11 (Extended Data Table 1). They show that all four bnAbs bind in a similar way (Fig. 1), interacting with both subunits and leaving a similar footprint on the sE dimer (Extended Data Fig. 1).

The antibody/antigen contacts are centred in a valley lined by the *b* strand on the domain II side, and by the '150 loop' of domain I of the adjacent subunit on the opposite side (Fig. 1), with the heavy chain contacting both N67 and N153 glycans across the E-dimer interface (Fig. 1a, e–g). The 150 loop spans residues 148–159, connecting β-strands E_0 and F_0 of domain I[14], and carries the N153 glycan. The total buried surface area per epitope ranges between 1,050 and 1,400 $Å^2$, and the surface complementarity coefficient[15] is between 0.67 and 0.74 (Extended Data Table 2), which are values typical for antibody/antigen complexes. The surface electrostatic potentials of epitope and paratopes are mildly charged (Extended Data Fig. 2), with a relatively complementary charge distribution. The EDE2 antibodies recognize sE essentially via the heavy chain, with the light chain involved only in contacts with the N153 glycan. The heavy chain buries nearly 85% of the total buried surface area—63% belonging to the long EDE2 CDR H3, which forms a protrusion matching the concave surface of the sE dimer. This protrusion is preformed in the antibody, as shown by the 1.7 Å resolution structure of the unliganded EDE2 A11 scFv (Extended Data Fig. 3), indicating no entropic cost for binding. In contrast, the EDE1 antibodies engage a substantial amount of light chain contacts from all three CDR and framework regions, contributing in total 40% in C8 and 47% in C10 of the buried surface area in the complex with sE. Although the germ lines are different between EDE1 C8 and C10 and the CDRs contribute

[1]Institut Pasteur, Département de Virologie, Unité de Virologie Structurale, 75724 Paris Cedex 15, France. [2]CNRS UMR 3569 Virologie, 75724 Paris Cedex 15, France. [3]Université Paris-Sud, Faculté des Sciences, 91405 Orsay, France. [4]Division of Immunology and Inflammation, Department of Medicine, Hammersmith Hospital Campus, Imperial College London, London W12 0NN, UK. [5]Institut Pasteur, Protéopôle, CNRS UMR 3528, 75724 Paris Cedex 15, France. [6]Synchrotron SOLEIL, L'Orme des Merisiers, Saint Aubin, BP48, 91192 Gif-sur-Yvette, France. [7]Institut Pasteur, Département de Virologie, Unité des Interactions Moléculaires Flavivirus-Hôtes, 75724 Paris Cedex 15, France. [8]Institut Pasteur, Département de Virologie, Unité de Pathogénie Virale, INSERM U1108, 75724 Paris Cedex 15, France. [9]Institut Pasteur de Guyane, BP 6010, 97306 Cayenne, French Guiana. [10]Dengue Hemorrhagic Fever Research Unit, Office for Research and Development, Faculty of Medicine, Siriraj Hospital, Mahidol University, Bangkok 10700, Thailand. †Present addresses: Institut Curie, 75248 Paris Cedex 05, France (C.M.K.); Altravax, Inc., 725 San Aleso Avenue, Suite 2, Sunnyvale, California 94085, USA (M.E.N.S.); U1157 INSERM GIP-CYROI, 97491 Saint Clotilde, La Réunion, France (P.De.); Institut Pasteur du Cambodge, 5 Monivong Boulevard, PO Box 983, Phnom Penh, Cambodia (P.Du.).
*These authors contributed equally to this work.

Table 1 | Germline analysis of bnAbs EDE1 and EDE2

Heavy chain	V-H allele	V-H diverg‡	V-H aa ch/tot§	J-H allele	D-H allele	CDR length [1:2:3]	BSA (%)	
							CDR [1:2:3]	[CDR:FWR]
EDE2 A11	IGHV3-74*01†	8.68%	14/98	IGHJ6*02	IGHD3-22*01	[8:8:26]‖ [5:17:24]¶	[6:11:62]‖ [6:13:61]¶	[79:3]‖ [80:3]¶
EDE2 B7	IGHV3-74*01	6.94%	9/98	IGHJ6*02	IGHD3-22*01	[8:8:26]‖ [5:17:24]¶	[2:11:63]‖ [2:14:62]¶	[76:8]‖ [78:6]¶
EDE1 C8	IGHV3-64D*06	6.94%	12/98	IGHJ6*02	IGHD2-21*01	[8:8:15]‖ [5:17:13]¶	[0:14:23]‖ [0:22:23]¶	[37:24]‖ [45:16]¶
EDE1 C10	IGHV1-3*01	2.78%	4/98	IGHJ4*02	IGHD4-17*01	[8:8:21]‖ [5:17:19]¶	[0:9:44]‖ [0:9:44]¶	[53:0]‖ [53:0]¶
Light chain	**V-L allele**	**V-L**	**V-L aa**	**J-L allele**		**CDR length [1:2:3]**	**BSA (%)**	
							CDR [1:2:3]	[CDR:FWR]
EDE2 A11	IGL2-23*01†	6.94%	14/98	IGLJ3*02†	—	[9:3:10]‖ [14:7:10]¶	[0:0:4]‖ [0:10:4]¶	[4:13]‖ [14:3]¶
EDE2 B7	IGLV2-23*01†	4.51%	10/98	IGLJ3*02†	—	[9:3:10]‖ [14:7:10]¶	[0:0:4]‖ [0:10:4]¶	[4:11]‖ [14:2]¶
EDE1 C8	IGKV3-11*01	5.02%	9/95	IGKJ2*01	—	[6:3:10]‖ [11:7:10]¶	[10:5:15]‖ [10:9:15]¶	[30:9]‖ [34:5]¶
EDE1 C10	IGLV2-14*01	3.82%	10/98	IGLJ3*02	—	[9:3:10]‖ [14:7:10]¶	[17:8:14]‖ [17:13:14]¶	[39:8]‖ [44:3]¶

V-H, J-H, D-H, V-L, J-L represent the putative *Homo sapiens* genes and alleles corresponding to the given bnAb, predicted by IMGT analysis (see Methods).
† Additional possibilities were also predicted by IMGT (not shown).
‡ Nucleotide (nt) divergence (diverg). The total length for all V-H and V-L alleles is 288 nucleotides except for EDE1 C8 V-L (279 nucleotides).
§ Number of amino-acid (aa) changes out of total V-H/V-L amino-acid length (ch/tot).
Buried surface area (BSA) for CDR and framework regions. Buried surface area per CDR or framework region (FWR) are shown as percentage of the total BSA of Fab or ScFv within the complex with DENV-2 sE. Buried surface areas are represented per individual H-CDRs [1:2:3] and L-CDRs [1:2:3] or as a sum for light/heavy chain CDRs and framework regions [CDR:FWR].
‖IMGT and ¶Kabat definitions of CDR and framework regions.

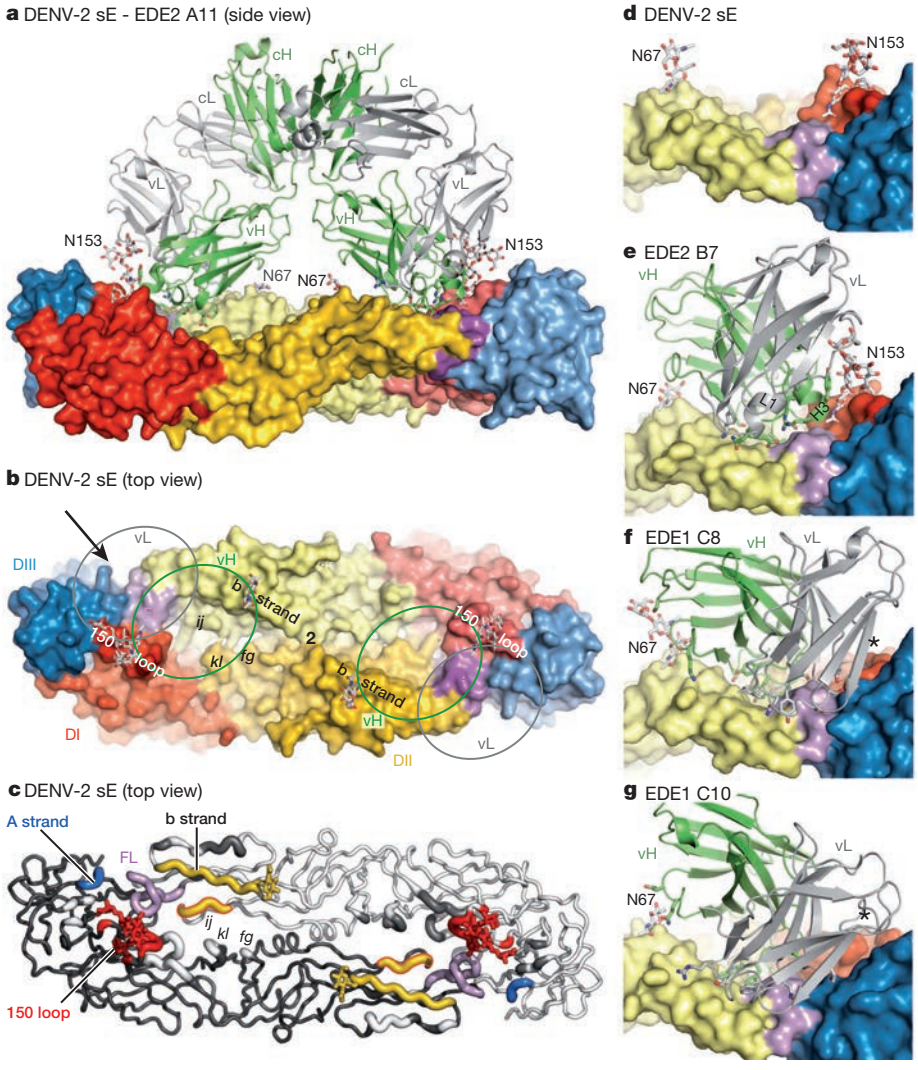

Figure 1 | DENV-2 sE in complex with four EDE bnAbs. **a**, Complex with Fab EDE2 A11. The sE dimer is in surface representation in side view, with the viral membrane-facing side below, coloured according to domains as labelled in **b**, with foreground and background subunits in bright and pale colours, respectively. The two N-linked glycan chains at N67 and N153 are shown as ball-and-stick and labelled. The A11 Fab is shown as ribbon with heavy and light chains in green and grey, respectively. **b**, The unliganded DENV-2 FGA02 sE dimer seen down the twofold axis (labelled '2'). Green and grey empty ovals (labelled vH and vL) show roughly the contact sites of heavy and light chains, respectively. Polypeptide segments relevant to the description of the epitopes are labelled. **c**, 'Worm' representation of the sE dimer, with the two subunits in different greys. Polypeptide segments in contact with the antibodies (either EDE1 or EDE2) are shown thicker, with the main segments of the epitope colour coded as boxed in Extended Data Fig. 4a, with additional contact segments in white or dark grey, depending on the subunit background. **d**, View down the arrow shown in **b**, highlighting the fusion loop 'valley' encased between two ridges, the *b* strand on one subunit and the 150 loop on the other. **e**–**g**, Same view as in **d** showing the complexes with bnAbs EDE2 B7 (**e**), EDE1 C8 (**f**) and EDE1 C10 (**g**) (only variable domains are shown). A black asterisk in **f** and **g** marks the region of the 150 loop, disordered in those complexes. Note that in the B7 and A11 complexes, the light chain is too far up to reach domain III.

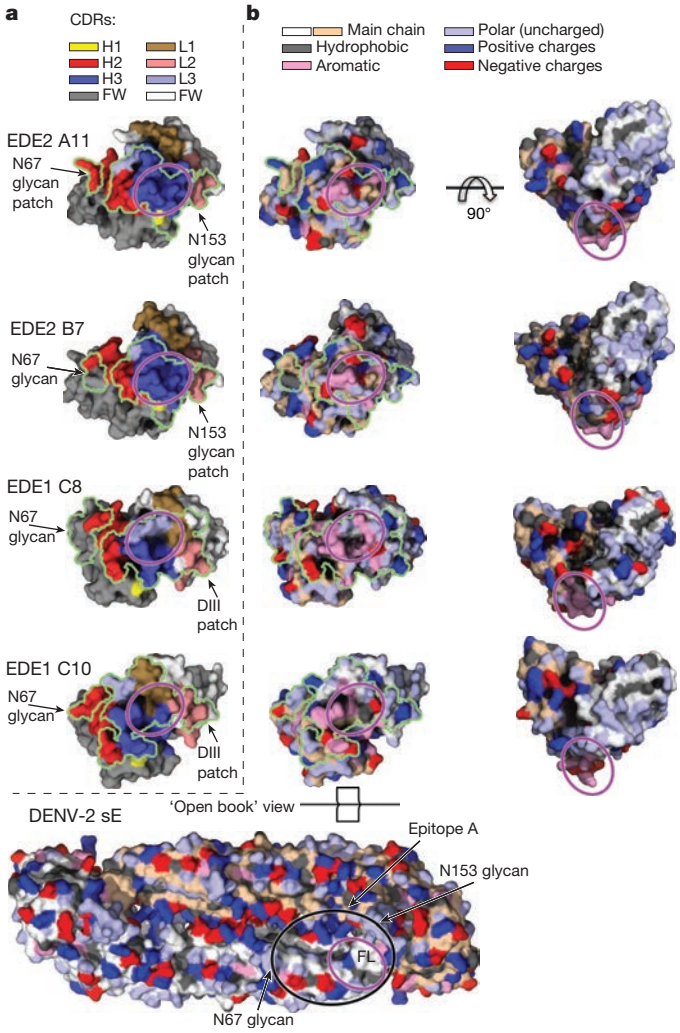

Figure 2 | Comparison of paratopes. **a**, The paratopes (outlined in green) on the antibody surface colour-coded by CDRs. The oval marks the region in contact with the E fusion loop. Note that the patch interacting with the N153 glycan (labelled) in EDE2 bnAbs corresponds to that interacting with domain III in EDE1 bnAbs. **b**, Chemical nature of paratope side chains. The left column corresponds to the same orientation as in **a**), with the surface coloured according to the side chain type. Exposed main-chain atoms of heavy and light chain are in sand and white, respectively. The bottom panel shows the sE dimer in the same rendering in an 'open book' orientation with respect to the antibodies. The epitope area is indicated with a black ellipse, with the fusion loop within the magenta oval corresponding to the one drawn on the antibodies.

differently to the paratope (Fig. 2a), the chemical nature of the residues involved is similar, including a clear clustering of aromatic side chains—a feature shared with the EDE2 bnAbs (Fig. 2b).

The bnAb contacts cluster on residues at the dimer interface (Fig. 1c) that are conserved across the four serotypes (Extended Data Fig. 4a), explaining their cross-reactivity. On domain II, both EDE1 and EDE2 bnAbs target the same residues (Extended Data Figs 4 and 5), which map to three main polypeptide segments: the *b* strand (amino acids 67–74, bearing the N67 glycan), the fusion loop and residues immediately upstream (amino acids 97–106), and the *ij* loop (amino acids 246–249). In contrast, on the opposite subunit the residues targeted are different: the EDE2 bnAbs interact with the 150 loop and the N153 glycan chain, whereas EDE1 bnAbs target domains I and III and induce disorder of the 150 loop. The structure of unliganded DENV-2 sE of the same strain (FGA-02, Fig. 1b–d), determined in parallel, was useful in assessing that EDE1 antibody binding indeed displaces the 150 loop. This is relevant because a previous structure of DENV-4 sE in complex with an antibody that binds away from the EDE also had the 150 loop disordered[13], highlighting an intrinsic mobility in this area depending on the E amino-acid sequence. Displacement of the 150 loop allows the EDE1 light chain to come closer to sE and interact with domain III (compare panel e with f and g in Fig. 1) in the region of the 'A strand' epitope, which has been structurally characterized previously for murine DENV cross-reactive antibodies[16,17]. These domain III contacts are centred on the conserved E residue K310, the side chain of which makes a lid covering the indole ring of W101 of the fusion loop (Extended Data Fig. 6a), in an important stabilizing E-dimer contact.

The bnAbs make extensive interactions with the glycan chains, both at positions N67 and N153 of protein E (Extended Data Figs 6 and 7), using opposite sides of the paratope (Fig. 2a). The complex of sE with EDE1 C8 displays the highest-ordered N67 glycan structure (Extended Data Fig. 7), with interactions with CDR H2 (Fig. 2a). The distal mannose residues contact the framework region 3 (framework H3; Extended Data Figs 4b and 7). Except for EDE1 C10 (which is very close to its germ line; Table 1), several framework H3 residues in the other bnAbs analysed have undergone changes (Extended Data Fig. 4b), suggesting affinity maturation to recognize the sugars. With respect to the N153 glycan, the structure of sE in complex with the EDE2 bnAbs displays clear electron density for the 6 sugar residues closest to the aparagine side chain (including in omit maps, as shown in Extended Data Fig. 7). A short α-helix in A11 and B7 CDR H3 projects aromatic side chains that pack against the sugar residues 1, 3 and 4 of the N153 glycan. The most distant residues of the glycan, mannoses 4, 5 and 6, are in contact with the light chain, via residues from CDR L2, including several hydrogen bonds (Extended Data Fig. 7 and Supplementary Information).

The glycine-rich fusion loop in the E dimer is such that it essentially exposes main-chain atoms, while the hydrophobic side chains are mostly buried. Together with the main chain of the *ij* loop, main-chain atoms make a large surface patch that is augmented by the exposed edge of the *b* strand (Fig. 3). The bnAbs make several specific hydrogen bonds to the sE main chain (Extended Data Fig. 6, see also list of interactions in Supplementary Information). Furthermore, the exposed side chains in this area are mostly conserved, resulting in a core region of the EDE that is serotype invariant, with non-conserved residues essentially at the periphery. The principal binding determinants of the EDE bnAbs thus appear to be the conformation of the main chain of the fusion

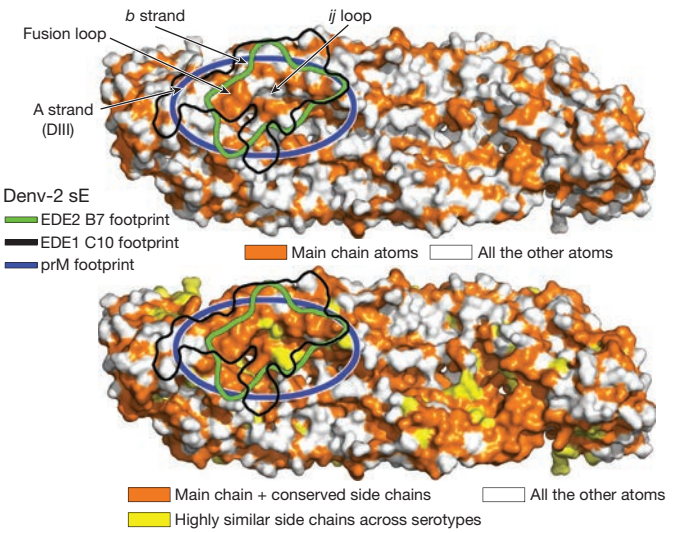

Figure 3 | Exposed main-chain atoms in the epitope. Surface representation of DENV-2 sE as viewed from outside the virion, with exposed main-chain atoms orange (top) or with main-chain atoms plus conserved side chains in orange, and highly similar side chains in yellow (bottom). The epitopes of EDE1 bnAb C10 (black outline) and EDE2 bnAb B7 (green outline) are indicated, with the prM footprint outlined in blue.

loop and its immediate neighbours in the context of an intact E dimer. This contrasts with the other major class of antibodies isolated from humans, which recognize the fusion loop sequence in a context independent of the quaternary organization[7]. The latter are cross reactive but poorly neutralizing and have a strong infection enhancing potential[18].

What is the reason for the strong conservation of this site across serotypes? In the infected cell, newly synthesized immature DENV virions bud into the endoplasmic reticulum lumen, where the pH is neutral. These particles contain 180 copies of a heterodimer of protein E with the precursor membrane glycoprotein prM at their surface[19,20]. As they are subsequently transported to the external medium across the Golgi apparatus, where the pH is acidic, the interaction with prM protects E from undergoing a premature acid-induced fusogenic conformational change[1]. The E/prM heterodimers reversibly associate as 60 trimers or 90 dimers at neutral or acidic pH, respectively[9,21]. Upon cleavage of its viral membrane tether by the TGN resident furin protease, prM remains bound to E dimers as long as the environment is acidic but it is released when the particle reaches the exterior of the cell (where the pH is neutral), thereby activating the virion to become fusogenic upon re-encountering the acidic endosomal environment of a new cell. The binding site of prM on the E dimer[9,21] maps precisely to the EDE (Fig. 3), explaining the high conservation of this site. As the E-dimer conformation with bound prM was observed on immature particles at low pH only[9], at neutral pH the EDE is not formed, and accordingly bnAbs do not bind to particles that are 100% immature[7], which are formed exclusively of E/prM trimers[19]. But the efficient binding of the bnAbs to particles that have more than 60% uncleaved prM[7], which have been shown to display patches of immature E/prM trimers at their surface[22,23], shows that these trimers must undergo a dynamic exchange with dimers. As the bnAbs have a higher affinity, they outcompete uncleaved prM on partly immature virions from its interaction with E dimers, binding by conformational selection[24]. This process effectively displaces the equilibrium towards dimers, similar to the bnAb-induced shift towards dimers of the sE monomer–dimer equilibrium in solution (data not shown). Because the degree of prM cleavage is variable and depends on the particular cell in which the virus was replicated, the fact that these bnAbs bind efficiently partly mature particles is expected to be important for protection in humans.

The EDE is totally circumscribed to the E dimer and therefore it does not depend on the higher-order arrangement of dimers, as recently suggested for other quaternary epitopes on the DENV particle[25] on the basis of studies on a different flavivirus, the West Nile virus[26]. Recent studies on DENV-2 detected a particle expansion at physiological temperatures of humans, causing the E dimers to reorient with respect to each other and presenting a different surface pattern as in mosquito-grown viruses[27,28]. bnAbs targeting the EDE will neutralize regardless of the surface arrangement of E dimers. These results are in line with a recent study on the tick-borne encephalitis flavivirus, in which the corresponding recombinant sE dimer efficiently depleted human serum from neutralizing activity[29].

As a corollary, our results suggest that, similar to vaccine approaches against the respiratory syncytial virus[30], a viable strategy would consist of presenting a single stabilized pre-fusion E dimer to the immune system, designed to focus the B-cell response on the EDE, instead of the multivalent vaccines that are currently under development.

Online Content Methods, along with any additional Extended Data display items and Source Data, are available in the online version of the paper; references unique to these sections appear only in the online paper.

Received 30 April; accepted 1 December 2014.

Published online 12 January 2015.

1. Lindenbach, B., Thiel, H. & Rice, C. *Flaviviridae: the Viruses and their Replication* 5th edn, Vol. 1, 1101–1152 (Lippincott Williams & Wilkins, 2007).
2. Bhatt, S. *et al.* The global distribution and burden of dengue. *Nature* **496,** 504–507 (2013).
3. Capeding, M. R. *et al.* Clinical efficacy and safety of a novel tetravalent dengue vaccine in healthy children in Asia: a phase 3, randomised, observer-masked, placebo-controlled trial. *Lancet* **384,** 1358–1365 (2014).
4. Normile, D. Tropical diseases. Dengue vaccine trial poses public health quandary. *Science* **345,** 367–368 (2014).
5. Fibriansah, G. *et al.* A potent anti-dengue human antibody preferentially recognizes the conformation of E protein monomers assembled on the virus surface. *EMBO Mol. Med.* **6,** 358–371 (2014).
6. Teoh, E. P. *et al.* The structural basis for serotype-specific neutralization of dengue virus by a human antibody. *Sci. Translat. Med.* **4,** 139–183 (2012).
7. Dejnirattisai, W. *et al.* A new class of highly potent broadly neutralizing antibodies isolated from dengue viremic patients. *Nature Immunol.* http://dx.doi.org/10.1038/ni.3058 (15, December 2014).
8. Modis, Y., Ogata, S., Clements, D. & Harrison, S. C. A ligand-binding pocket in the dengue virus envelope glycoprotein. *Proc. Natl Acad. Sci. USA* **100,** 6986–6991 (2003).
9. Yu, I. M. *et al.* Structure of the immature dengue virus at low pH primes proteolytic maturation. *Science* **319,** 1834–1837 (2008).
10. Kuhn, R. J. *et al.* Structure of dengue virus: implications for flavivirus organization, maturation, and fusion. *Cell* **108,** 717–725 (2002).
11. Zhang, X. *et al.* Cryo-EM structure of the mature dengue virus at 3.5-A resolution. *Nature Struct. Mol. Biol.* **20,** 105–110 (2013).
12. Zhang, Y. *et al.* Conformational changes of the flavivirus E glycoprotein. *Structure* **12,** 1607–1618 (2004).
13. Cockburn, J. J. *et al.* Structural insights into the neutralization mechanism of a higher primate antibody against dengue virus. *EMBO J.* **31,** 767–779 (2012).
14. Rey, F. A., Heinz, F. X., Mandl, C., Kunz, C. & Harrison, S. C. The envelope glycoprotein from tick-borne encephalitis virus at 2 Å resolution. *Nature* **375,** 291–298 (1995).
15. Lawrence, M. C. & Colman, P. M. Shape complementarity at protein/protein interfaces. *J. Mol. Biol.* **234,** 946–950 (1993).
16. Cockburn, J. J. *et al.* Mechanism of dengue virus broad cross-neutralization by a monoclonal antibody. *Structure* **20,** 303–314 (2012).
17. Lok, S. M. *et al.* Binding of a neutralizing antibody to dengue virus alters the arrangement of surface glycoproteins. *Nature Struct. Mol. Biol.* **15,** 312–317 (2008).
18. Rodenhuis-Zybert, I. A. *et al.* A fusion-loop antibody enhances the infectious properties of immature flavivirus particles. *J. Virol.* **85,** 11800–11808 (2011).
19. Zhang, Y. *et al.* Structures of immature flavivirus particles. *EMBO J.* **22,** 2604–2613 (2003).
20. Kostyuchenko, V. A., Zhang, Q., Tan, J. L., Ng, T. S. & Lok, S. M. Immature and mature dengue serotype 1 virus structures provide insight into the maturation process. *J. Virol.* **87,** 7700–7707 (2013).
21. Li, L. *et al.* The flavivirus precursor membrane-envelope protein complex: structure and maturation. *Science* **319,** 1830–1834 (2008).
22. Plevka, P. *et al.* Maturation of flaviviruses starts from one or more icosahedrally independent nucleation centres. *EMBO Rep.* **12,** 602–606 (2011).
23. Plevka, P., Battisti, A. J., Sheng, J. & Rossmann, M. G. Mechanism for maturation-related reorganization of flavivirus glycoproteins. *J. Struct. Biol.* **185,** 27–31 (2014).
24. Changeux, J. P. & Edelstein, S. Conformational selection or induced fit? 50 years of debate resolved. *F1000 Biol. Rep.* **3,** 19 (2011).
25. de Alwis, R. *et al.* Identification of human neutralizing antibodies that bind to complex epitopes on dengue virions. *Proc. Natl Acad. Sci. USA* **109,** 7439–7444 (2012).
26. Kaufmann, B. *et al.* Neutralization of West Nile virus by cross-linking of its surface proteins with Fab fragments of the human monoclonal antibody CR4354. *Proc. Natl Acad. Sci. USA* **107,** 18950–18955 (2010).
27. Fibriansah, G. *et al.* Structural changes of dengue virus when exposed to 37°C. *J. Virol.* **87,** 7585–7592 (2013).
28. Zhang, X. *et al.* Dengue structure differs at the temperatures of its human and mosquito hosts. *Proc. Natl Acad. Sci. USA* **110,** 6795–6799 (2013).
29. Jarmer, J. *et al.* Variation of the specificity of the human antibody responses after tick-borne encephalitis virus infection and vaccination. *J. Virol.* **88,** 13845–13857 (2014).
30. McLellan, J. S. *et al.* Structure-based design of a fusion glycoprotein vaccine for respiratory syncytial virus. *Science* **342,** 592–598 (2013).

Supplementary Information is available in the online version of the paper.

Acknowledgements This work was made possible by a Pediatrics Dengue Vaccine Initiative grant to F.A.R., allowing the set up of a production facility of recombinant DENV sE. The co-crystallization with the bnAbs was done with European Union funding (DenFree consortium) to F.A.R. and G.R.S./J.M. F.A.R. acknowledges support from Insitut Pasteur, from the French Government's 'Investissements d'Avenir' program: Laboratoire d'Excellence 'Integrative Biology of Emerging Infectious Diseases' (grant number ANR-10-LABX-62-IBEID) and the CNRS. G.S.R. and J.M. were supported by the Medical Research Council, UK, the Wellcome Trust, UK, the National Institute for Health Research Biomedical Research Centre, Funding Scheme. G.R.S. is a Wellcome Trust Senior investigator. We thank staffs at beam lines PROXIMA-1 and PROXIMA-2 at the SOLEIL synchrotron (St Aubin, France) and ID23-2 and ID29 at the European Synchrotron Radiation Facility (Grenoble, France). We thank A. Sakuntabhai for coordination of the DenFree grant, G. Bricogne for advice on diffraction data collection strategies, J. Cockburn and P.-Y. Lozach for help with the initial sE constructs, and S. Halstead and S. Kliks for support through the Pediatrics Dengue Vaccine Initiative.

Author Contributions J.M., G.R.S. and F.A.R. conceived the experiments. W.W. and W.D. made the constructs for production of antibody fragments in S2 cells. M.E.N.S. and C.M.K. made the constructs for production of recombinant sE, and crystallized the unliganded form of DENV-2 FGA02 sE. C.G.B. and S.P. produced large amounts of sE

protein for crystallization. A.R. and G.B.S. prepared the recombinant bnAb fragments and sE for crystallization. A.R. and A.H. optimized the crystals of the complexes. P.G.C., W.E.S., S.D., M.C.V. and A.R. collected and processed the diffraction data. P.G.C., M.C.V. and S.D. determined the structures and refined the atomic models. P.De., F.A.S. and F.A.R. conceived the protocols for production of recombinant sE. P.Du. provided a plasmid containing the envelope protein of DENV-2 FGA02 strain circulating in French Guiana in 2002. F.A.R. wrote the paper with the help of A.R., P.G.C., G.B.S., M.C.V. and S.D.

Author Information Coordinates and structure factor amplitudes have been deposited in the Protein Data Bank under accession numbers 4UTC, 4UTA, 4UT9, 4UTB and 4UT6 respectively for the structures of DENV-2 sE unliganded and in complex with EDE1 C8, EDE1 C10, EDE2 A11 and EDE2 B7, and 4UT7 for the structure of the unliganded scFv of EDE2 A11. The sequence of prM/sE fragment from Den2_FGA-02 has been deposited in GenBank under accession number KM087965. Patent application (UK 1413086.8) was deposited. Reprints and permissions information is available at www.nature.com/reprints. The authors declare no competing financial interests. Readers are welcome to comment on the online version of the paper.
Correspondence and requests for materials should be addressed to F.A.R. (rey@pasteur.fr), G.R.S. (g.screaton@imperial.ac.uk) or J.M. (j.mongkolsapaya@imperial.ac.uk).

METHODS

No statistical methods were used to predetermine sample size.

Recombinant sE protein production. Recombinant DENV-2 FGA02 sE (1-395) was cloned into a vector pMT/BIP/V5-His with a carboxy (C)-terminal His-tag and produced in *Drosophila* S2 cells[31], performed essentially as described earlier for DENV-4 sE (Den4_Burma/63632/1976)[13], with some modifications (see below). Briefly, sE expression was driven by the metallothionein promoter and was induced by 5 μM of $CdCl_2$ in Insect-XPRESS medium (Lonza). The constructs had a *Drosophila* BiP signal sequence fused at the amino (N)-terminal end of a prM/sE construct for efficient translocation into the endoplasmic reticulum of the transfected S2 cells. prM was present N-terminal to sE, as in the DENV polyprotein precursor, with the N termini of prM and sE generated by signalase cleavage in the endoplasmic reticulum, where prM (which remains membrane-anchored) plays a chaperone role by masking the fusion loop of sE. The prM/sE complex is transported across the acidic compartments, where prM is cleaved by furin into pr (N-terminal half, bound to sE) and M (membrane-anchored C-terminal half). Upon reaching the external milieu, sE and pr dissociate, and the sE component is purified by affinity chromatography from the cells' supernatant fluid. Clarified cell supernatants were concentrated 20-fold using Vivaflow tangential filtration cassettes (Sartorius, cut-off 10 kDa) and adjusted to pH 8.0, Tris 20 mM and 500 mM NaCl before purification in an AKTA FPLC system by HisTrap-HP chromatography. The protein was de-salted after elution of the HisTrap column and further purified by ion exchange chromatography on MonoQ. A final purification gel filtration step used a Superdex 200 10/300 GL column equilibrated in 50 mM Tris pH8, 500 mM NaCl.

Note that the last four residues (392–395) were inadvertently replaced by a 'vector' sequence 'LRPL' instead of 'FKKG' as in the correct DENV-2 sequence (see Extended Data Fig. 4a). Fortunately, the 'vector' residues correctly completed the β-strand G of domain III and did not introduce any detectable difference in conformation there compared with the other available structures of DENV-2 sE. This discrepancy in the amino-acid sequence has been explicitly indicated in the deposited Protein Data Bank file.

Production of antigen-binding (Fab) and single-chain Fv (scFv) fragments of the bnAbs. The bnAb fragments were cloned into plasmids for expression as Fab[32] and scFv[31] in *Drosophila* S2 cells. The constructs contain a twin strep tag fused at the C terminus (only of the heavy chain in the case of the Fab) for affinity purification. The purification protocol included a streptactin affinity column followed by gel filtration as described above.

Immune complex formation and isolation. The purified DENV-2 sE protein was mixed with Fabs or ScFvs (in approximately twofold molar excess) in standard buffer (500 mM NaCl, Tris 50 mM pH 8.0). The volume was brought to 0.2 ml by centrifugation in a Vivaspin 10 kDa cutoff; after 30 min incubation at 4 °C, the complex was separated from excess Fab or scFv by size-exclusion chromatography except when a clear peak for the complex was not obtained. In this case, a molar ratio 1:2 antigen:antibody mixture (that is, with an excess of antibody) was directly used for crystallization. In all cases, the buffer was exchanged to 150 mM NaCl, 15 mM Tris, pH 8 for crystallization trials. The protein concentrations used for crystallization, determined by measuring the absorbance at 280 nm and using an extinction coefficient estimated from the amino-acid sequences, are listed in Extended Data Table 1.

Crystallization and three-dimensional structure determinations. Crystallization trials were performed in sitting drops of 400 nl. Drops were formed by mixing equal volumes of the protein and reservoir solution in the format of 96 Greiner plates, using a Mosquito robot, and monitored by a Rock-Imager. Crystals were optimized with a robotized Matrix Maker and Mosquito setups on 400 nl sitting drops, or manually in 24-well plates using 2–3 μl hanging drops. The crystallization and cryo-cooling conditions for diffraction data collection are listed in Extended Data Table 1.

X-ray diffraction data were collected at beam lines PROXIMA-1 and PROXIMA-2 at the SOLEIL synchrotron (St Aubin, France), and ID23-2 and ID29 at the European Synchrotron Radiation Facility (Grenoble, France) (Extended Data Table 1). Diffraction data were processed using the XDS package[33] and scaled with SCALA or AIMLESS[34] in conjunction with other programs of the CCP4 suite[35]. The structures were determined by molecular replacement with PHASER[36] and/or AMoRe[37] using the search models listed in Extended Data Table 1.

Subsequently, careful model building with COOT[38], alternating with cycles of crystallographic refinement with the program BUSTER/TNT[39], led to a final model. Refinement was constrained to respect non-crystallographic symmetry, and used target restraints (with high-resolution structures of parts of the complexes) and TLS refinement[40] depending on the resolution of the crystal (see Extended Data Table 1). Final omit maps were calculated using Phenix.Refine[41] (Extended Data Fig. 7).

Analysis of the atomic models and Illustrations. Each complex was analysed with the CCP4 suite of programs[35]. For intermolecular interactions, the maximal cutoff distance used for the interactions was 4.75 Å. Then the contacts of each residue of the Fab/ScFv or of DENV sE proteins were counted and plotted as a proportional bar above the corresponding residue.

The Ab sequences were analysed by Abysis (http://www.bioinf.org.uk/software) and IMGT (http://www.imgt.org)[42] websites for mapping CDR/framework regions according to Kabat[43] and IMGT[42]conventions, respectively. The analysis of the putative germline and somatic maturation events was done with the IMGT website (www.imgt.org).

Multiple sequence alignments were calculated using Clustal W and Clustal X version 2 (ref. 44) on the EBI server[45]. The figures were prepared using ESPript[46] and the PyMOL Molecular Graphics System, version 1.5.0.4 (Schrödinger) (pymol.sourceforge.net) with APBS[47] and PDB2PQR tools[48]. For analysis, we created an atomic model for the DENV-2 sE dimer on the basis of chain A of sE from the complex with B7 (PDB 4UT6), which had no density breaks, to calculate the surface of the sE dimer presented in the corresponding panels in Figs 2b and 3 and Extended Data Fig. 2.

31. Gilmartin, A. A. *et al.* High-level secretion of recombinant monomeric murine and human single-chain Fv antibodies from *Drosophila* S2 cells. *Protein Eng. Des. Sel.* **25,** 59–66 (2012).
32. Backovic, M. *et al.* Efficient method for production of high yields of Fab fragments in *Drosophila* S2 cells. *Protein Eng. Des. Sel.* **23,** 169–174 (2010).
33. Kabsch, W. XDS. *Acta Crystallogr. D* **66,** 125–132 (2010).
34. Evans, P. R. & Murshudov, G. N. How good are my data and what is the resolution? *Acta Crystallogr. D* **69,** 1204–1214 (2013).
35. Winn, M. D. *et al.* Overview of the CCP4 suite and current developments. *Acta Crystallogr. D* **67,** 235–242 (2011).
36. McCoy, A. J. *et al.* Phaser crystallographic software. *J. Appl. Cryst.* **40,** 658–674 (2007).
37. Navaza, J. Implementation of molecular replacement in AMoRe. *Acta Crystallogr. D* **57,** 1367–1372 (2001).
38. Emsley, P., Lohkamp, B., Scott, W. G. & Cowtan, K. Features and development of Coot. *Acta Crystallogr. D* **66,** 486–501 (2010).
39. Blanc, E. *et al.* Refinement of severely incomplete structures with maximum likelihood in BUSTER-TNT. *Acta Crystallogr. D* **60,** 2210–2221 (2004).
40. Winn, M. D., Murshudov, G. N. & Papiz, M. Z. Macromolecular TLS refinement in REFMAC at moderate resolutions. *Methods Enzymol.* **374,** 300–321 (2003).
41. Afonine, P. V. *et al.* Towards automated crystallographic structure refinement with *phenix.refine*. *Acta Crystallogr. D* **68,** 352–367 (2012).
42. Lefranc, M. P. *et al.* IMGT, the international ImMunoGeneTics information system. *Nucleic Acids Res.* **37,** D1006–D1012 (2009).
43. Wu, T. T. & Kabat, E. A. An analysis of the sequences of the variable regions of Bence Jones proteins and myeloma light chains and their implications for antibody complementarity. *J. Exp. Med.* **132,** 211–250 (1970).
44. Larkin, M. A. *et al.* Clustal W and Clustal X version 2.0. *Bioinformatics* **23,** 2947–2948 (2007).
45. Goujon, M. *et al.* A new bioinformatics analysis tools framework at EMBL-EBI. *Nucleic Acids Res.* **38,** W695–699 (2010).
46. Gouet, P., Courcelle, E., Stuart, D. I. & Metoz, F. ESPript: analysis of multiple sequence alignments in PostScript. *Bioinformatics* **15,** 305–308 (1999).
47. Baker, N. A., Sept, D., Joseph, S., Holst, M. J. & McCammon, J. A. Electrostatics of nanosystems: application to microtubules and the ribosome. *Proc. Natl Acad. Sci. USA* **98,** 10037–10041 (2001).
48. Dolinsky, T. J., Nielsen, J. E., McCammon, J. A. & Baker, N. A. PDB2PQR: an automated pipeline for the setup of Poisson-Boltzmann electrostatics calculations. *Nucleic Acids Res.* **32,** W665–W667 (2004).
49. Chen, V. B. *et al.* MolProbity: all-atom structure validation for macromolecular crystallography. *Acta Crystallogr. D* **66,** 12–21 (2010).

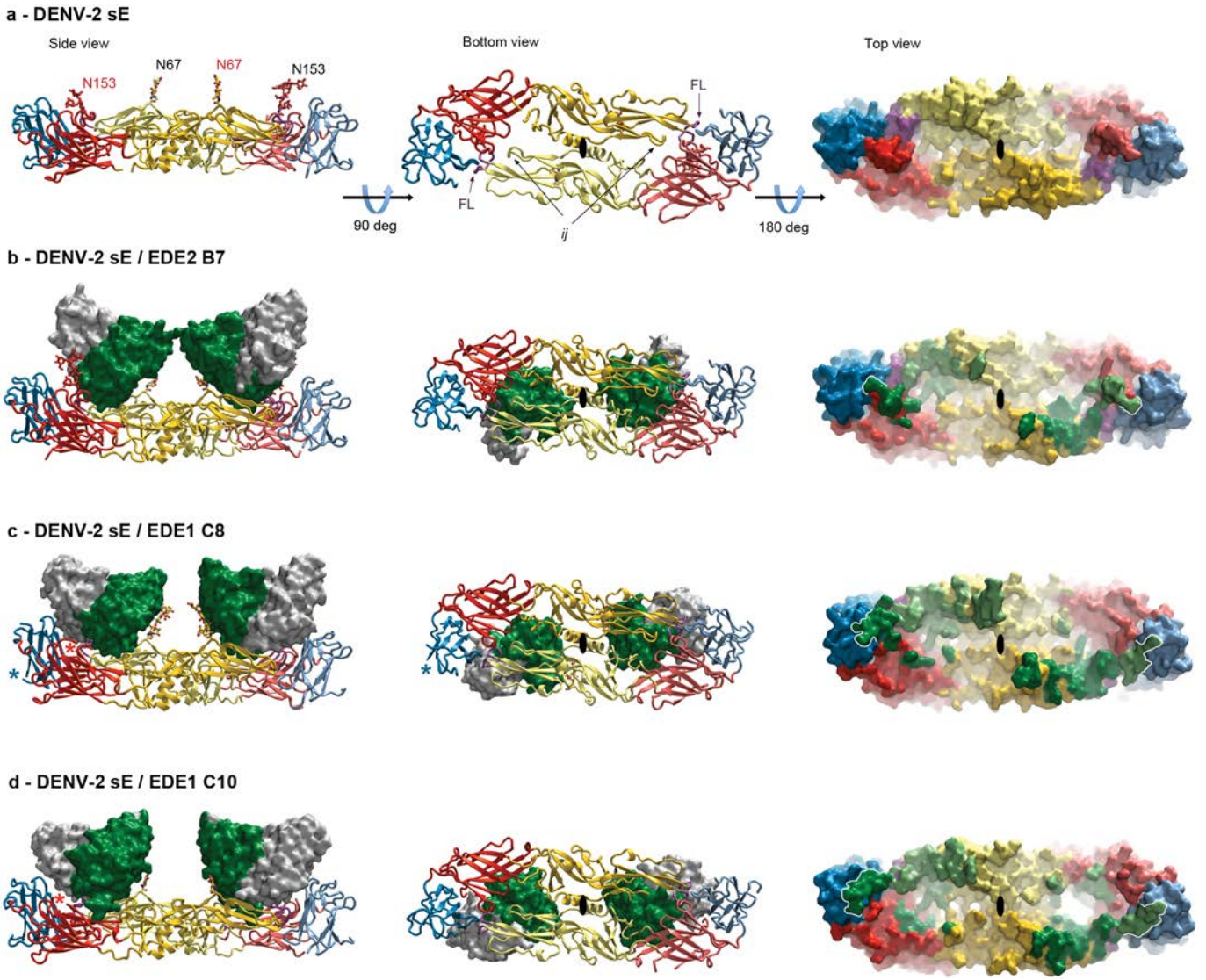

Extended Data Figure 1 | Overall complexes and footprints of the bnAbs on the sE dimer. **a**–**d**, Each row corresponds to a different sE/bnAb complex (except for the first one, which shows the unliganded sE dimer) and each column displays the same orientation, as labelled. In the first two columns the sE dimer is depicted as ribbons and the bnAb variable domains as surface coloured as in Fig. 1. In the side view (left column) the viral membrane would be underneath, whereas the bottom view (middle column) corresponds to the sE dimer seen from the viral membrane with the antibodies visible across the sE ribbons. The top view (right column) shows the sE surface as presented to the immune system on the viral particle, showing the footprint of the antibodies (green) with a white depth-cuing fog. For clarity, a white outline delimits the green footprint on the blue surface of domain III. As a guide, in the top-left panel the glycan chains of foreground and background subunits are labelled in red and black respectively. In the middle and right columns, the two-fold axis of the sE dimer is marked by a black ellipse at the centre. The fusion loop and the *ij* loop are labelled on the top-middle panel, and can be seen in the other rows in contact with the bnAbs. A red star in the left panels of rows **c** and **d** marks the location of the 150 loop, which is disordered in the complexes with the EDE1 bnAbs. This loop bears the N153 glycan recognized by the EDE2 bnAbs, as seen in row **b**, left panel (glycan shown as sticks with carbon atoms coloured red). In contrast, all the bnAbs are seen contacting the N67 glycan, with C8 displaying the most contacts (row **c**, left panel, N67 glycan as sticks with carbon atoms yellow). A blue star in row **c** shows a disordered loop in domain III. Note that EDE1 C10 (row **d**) inserts deeper into the sE dimer than the others bnAbs.

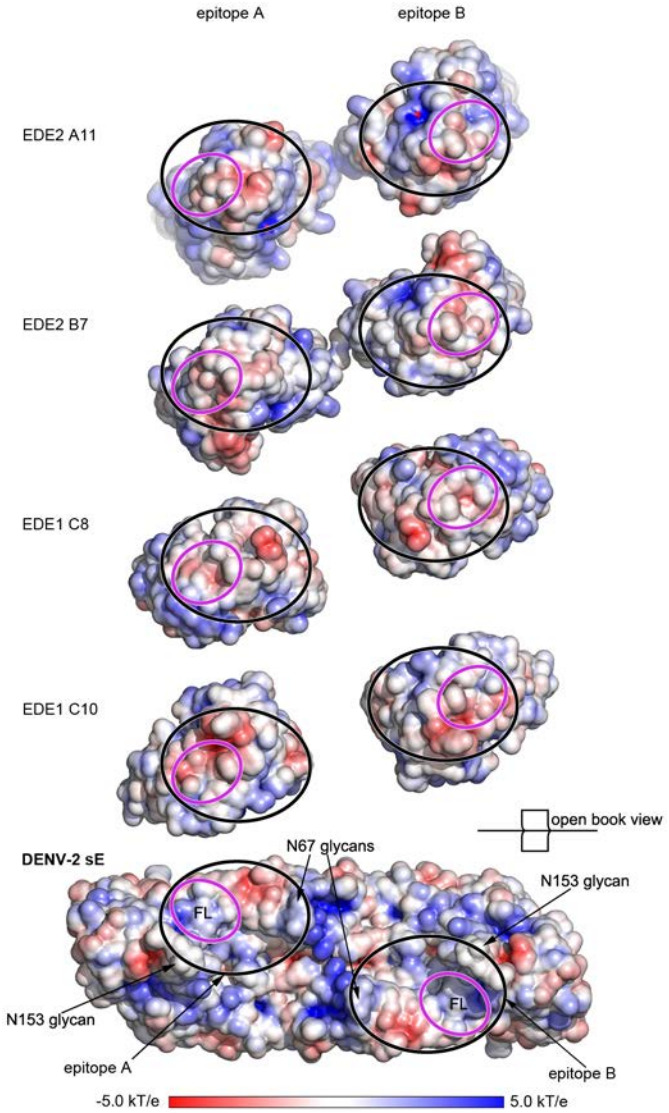

Extended Data Figure 2 | Electrostatic potential of paratopes and epitope. 'Open book' representation of the complexes, with negative and positive potential displayed and coloured according to the bar underneath. Because certain regions are disordered in the complexes, the unliganded DENV-2 sE dimer model, generated as described in the Methods section, was used to calculate the surface electrostatic potential of the sE dimer. Corresponding areas in contact are indicated by ovals as in Fig. 2.

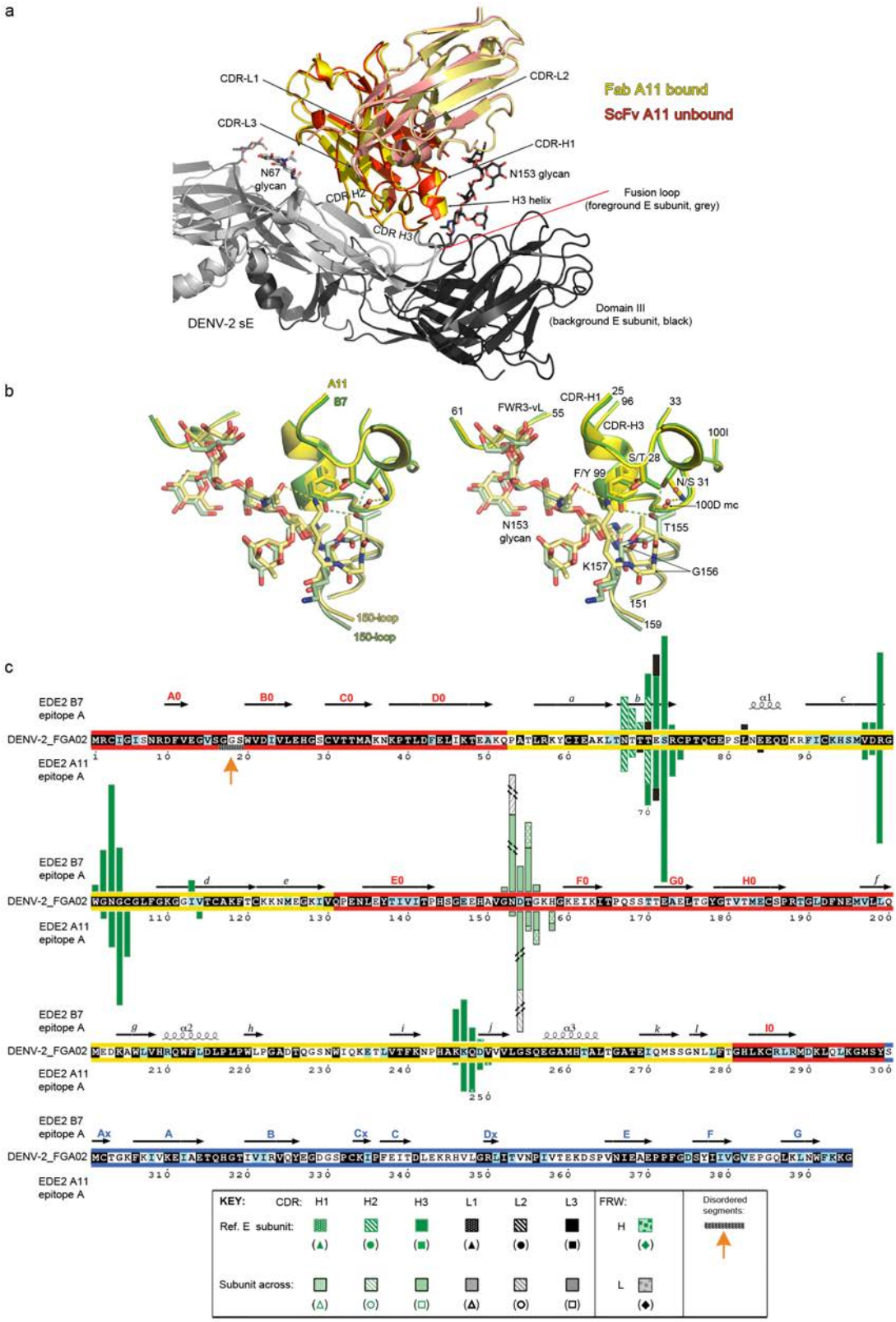

Extended Data Figure 3 | Unliganded bnAb A11 and EDE2 bnAbs in interactions with DENV-2 sE. **a**, The structure of the unliganded EDE2 A11 scFv (red, 1.7 Å resolution) superposed to the variable domain of Fab A11 in complex with DENV-2 sE (yellow, 3.8 Å resolution), to show that the same conformation is retained in the sE/Fab fragment complex. **b**, Stereo view showing the superposed B7 (green) and A11 (yellow) variable domains, together with the 150 loop extracted from the structures of the corresponding Fab/DENV-2 sE complexes. Note that the main chain of the 150 loop adopts different conformations in the two complexes, mainly because of the hydroxyl group the Y99 side chain in the CDR H3 of B7 makes a hydrogen bond with sE T155. A11 has a phenylalanine at this position, and so lacks the hydroxyl group. The sE protein in the complex with A11 displays the same conformation as the unliganded sE (not shown). **c**, Histograms of the atomic contacts of B7 (above the sE sequence) and A11 (below the sequence) according to the key at the bottom (see also detailed data and explanations in Supplementary Information). The secondary structure elements of the

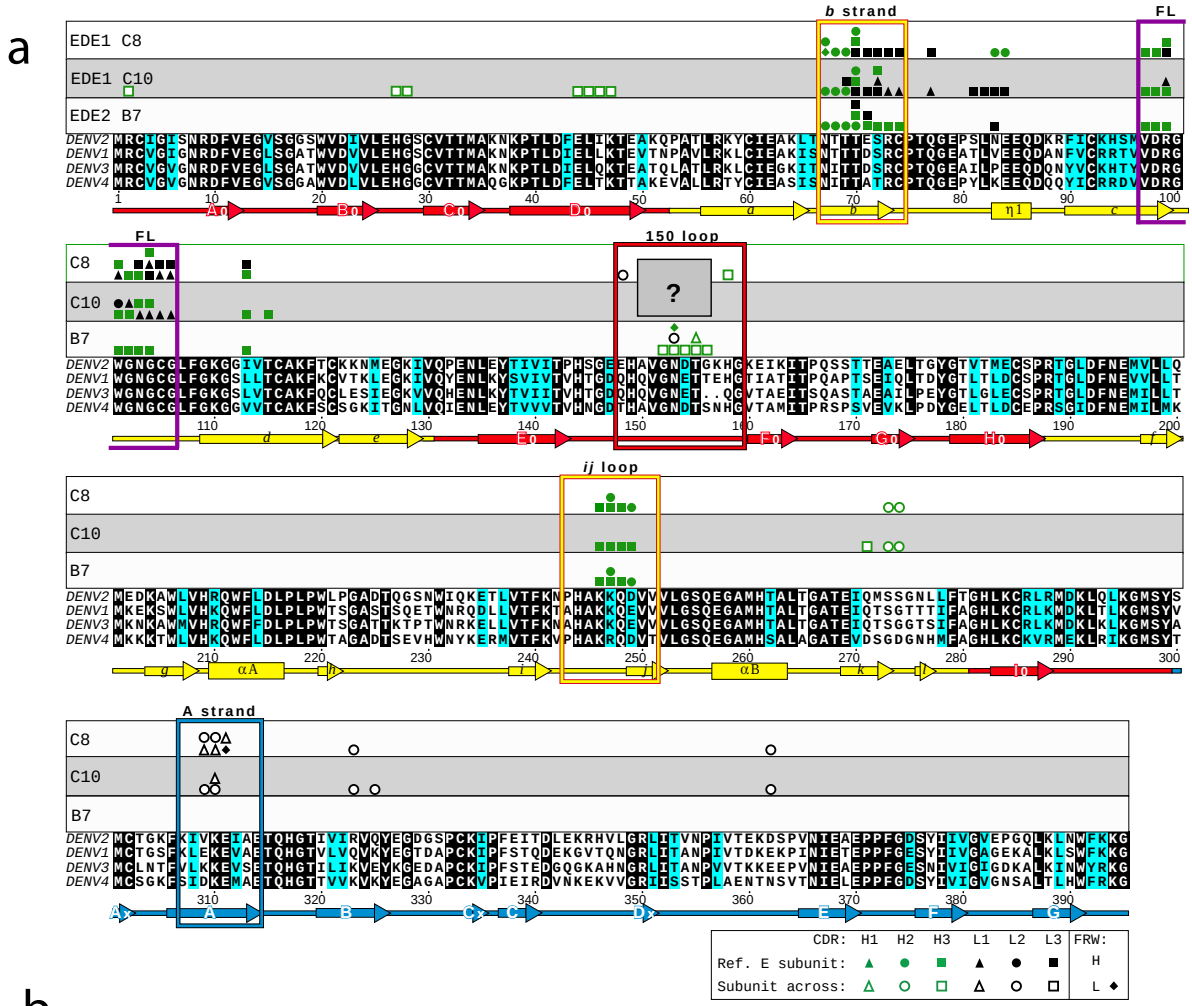

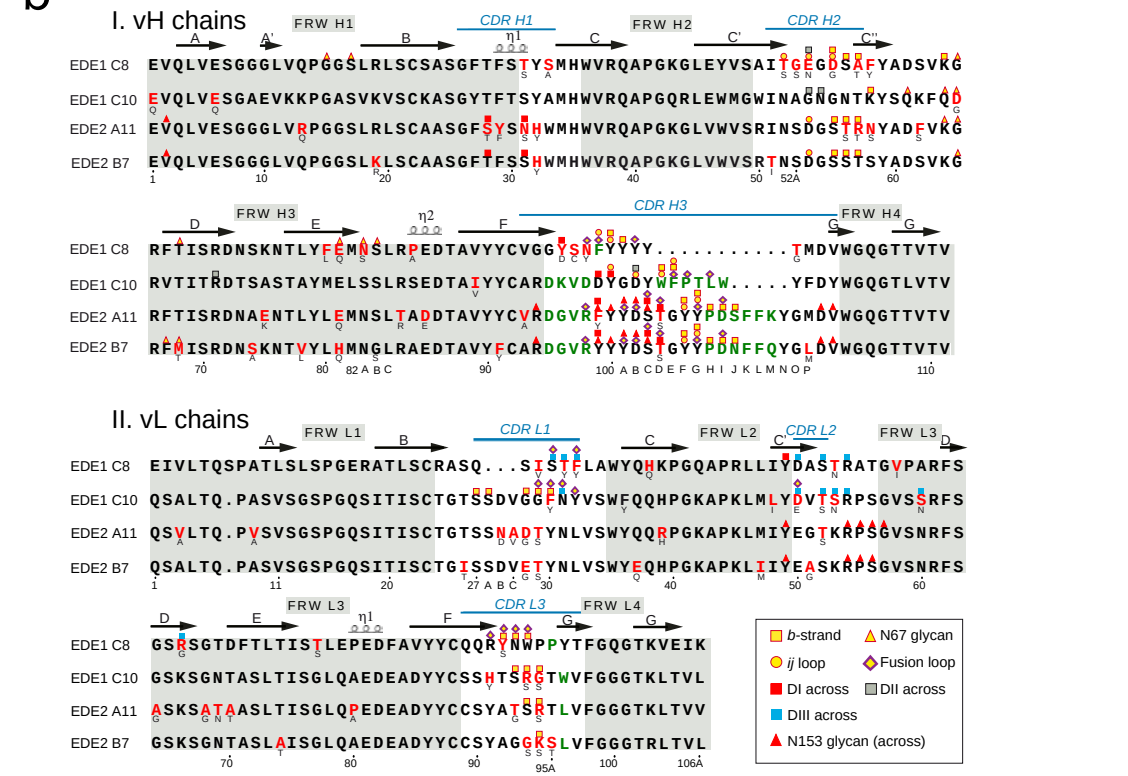

Extended Data Figure 4 | Residues involved in bnAb/antigen interactions. **a**, Amino-acid sequence alignment of sE from the four DENV serotypes, with residues in black or light blue background highlighting identity and similarity, respectively, across serotypes. Secondary structure elements are indicated underneath, with tertiary organization given by colours as in Fig. 1. DENV-2 sE residues contacted by the bnAbs are marked above, according to the code of the key (bottom-right insert). Full and empty symbols correspond to contacts on the reference subunit (defined as the one contributing the fusion loop to the epitope) and opposite subunit, respectively. Coloured boxes highlight the five distinct regions of sE making up the epitopes, matching Fig. 1c. The histogram displaying the number of atomic contacts per sE residue by each bnAb is provided as Supplementary Information. Because the EDE2 B7 and A11 contacts are very similar, only the B7 contacts are shown here. The question mark on the 150 loop indicates residues likely to contact the EDE1 bnAbs, but which are not visible in the structure because the loop is disordered. **b**, Sequence alignment of the four bnAbs crystallized and with the framework and CDR regions in grey and white background (in Kabat numbering[43]), respectively. Blue lines over the sequence mark the CDRs in the IMGT convention[42]. Somatic mutations are in red with germline residues in smaller font underneath. Residues arising from the recombination process are in green. A symbol above the sequence indicates the sE segment contacted, according to the key of the bottom-right inset. The secondary structure elements of the EDE1 C8 Ig β-barrels are indicated above the sequence, as guide.

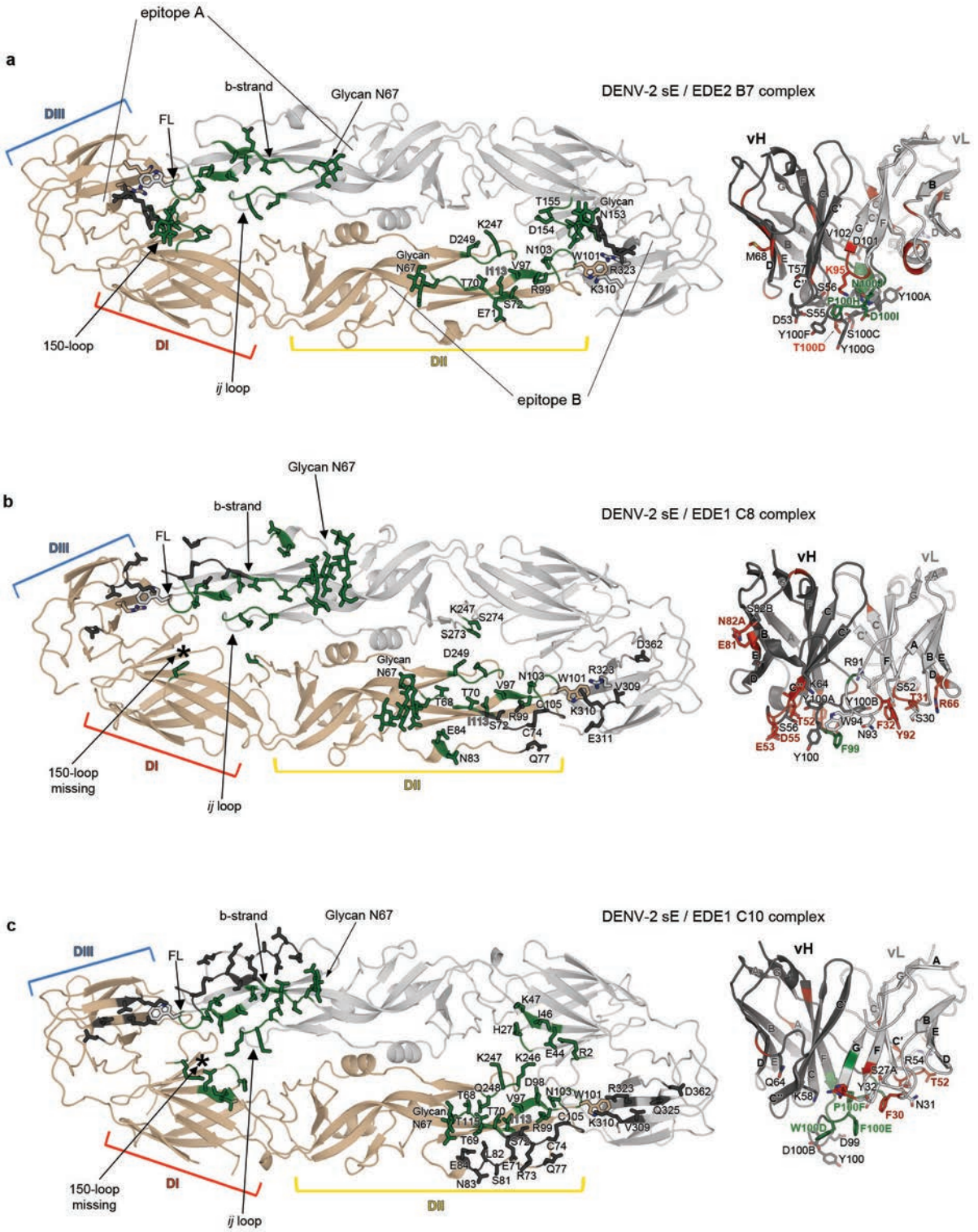

Extended Data Figure 5 | Epitopes and paratopes. The epitope area of DENV-2 sE from three different complexes is highlighted in green and dark grey, with relevant side chains as sticks, corresponding to residues interacting with the heavy and light chain, respectively (left panels). The variable domain of the corresponding bnAb is shown in side view, with interacting side chains labelled. Heavy and light chains are in dark and light grey, respectively, with somatic mutations in red and residues that arose through the recombination process (third CDR in each chain) in green. **a**, EDE2 B7 complex; **b**, EDE1 C8 complex; **c**, EDE1 C10 complex.

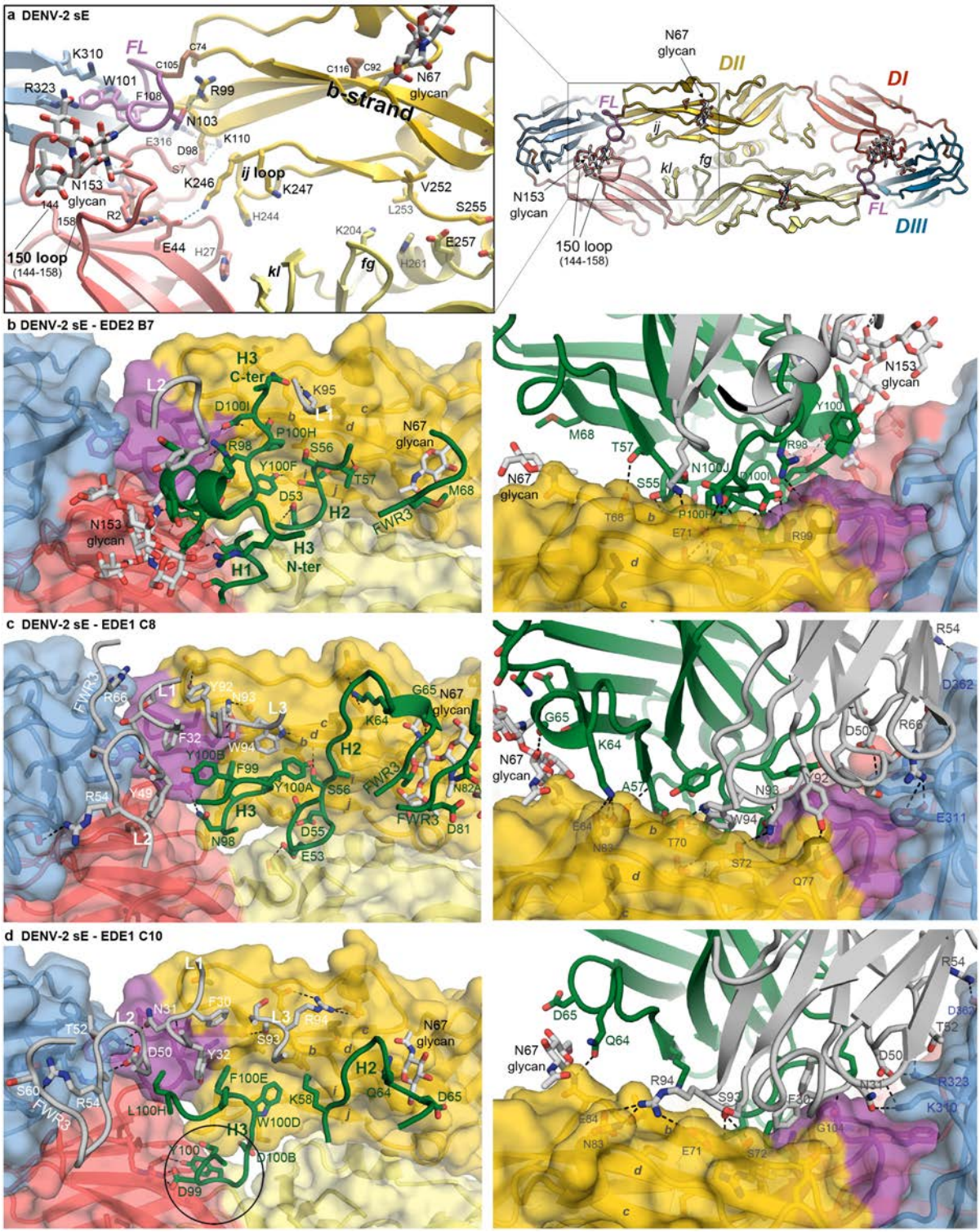

Extended Data Figure 6 | Key interactions of the bnAbs with sE. **a**, The right panel shows the sE dimer in ribbons, with the framed area enlarged in the left panel to show the epitope, with main features labelled. **b**, sE dimer in complex with bnAb EDE2 B7, **c** with EDE1 C8 and **d** with EDE1 C10. The sE dimer surface is shown in a semi-transparent representation with the ribbons visible through. The glycan residues were not included in the surface, and are displayed as sticks. The relevant CDR loops of the bnAbs are shown as ribbons with side chains as sticks on top of the sE protein, coloured as in Fig. 1. The orientation of the left panel in rows b–d corresponds to the enlargement of row a, and the right panel is a view along the arrow in Fig. 1b (main text). Hydrogen bonds are displayed as dotted lines. The circle in the left panel of **d** highlights a deep contact of EDE1 C10 CDR-H3 into the DENV-2 sE dimer (see also Extended Data Fig. 1d, left panel).

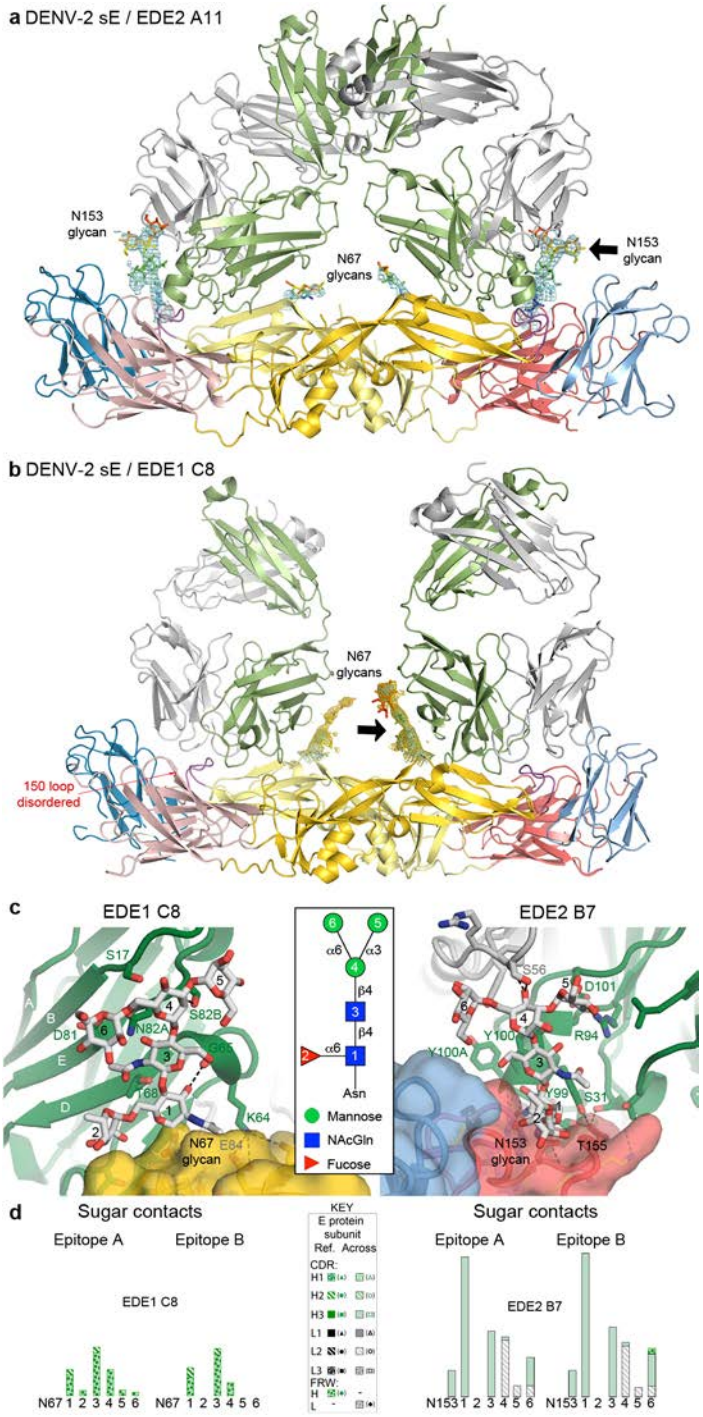

Extended Data Figure 7 | Interactions with the glycan chains. Ribbon representation of **a** the EDE2 A11 Fab and **b** the EDE1 C8 Fab in complex with DENV-2 sE, coloured as in Fig. 1. The simulated annealing omit maps contoured at 1σ (cyan) or 0.6σ (gold) show clear density for the N153 (in **a**) and N67 glycans (in **a** and **b**) (black arrows). To create an unbiased map, all glycan atoms were removed from the structures, all B factors were reset to 20 Å and the structures were re-refined using torsion dynamics simulated annealing. Note that the antibody spans the two glycans across the dimer interface (as also shown in Fig. 1). **c**, Views down the black arrow in **a** (left panel) and the arrow in **b** (right panel), through the glycan chain. The key to the sugar connectivity and nomenclature is framed at the centre. **d**, Contacts of the sugar residues with the antibodies, coded according to the key.

Extended Data Table 1 | Crystallization conditions, data collection and refinement statistics

Crystal	DENV-2 sE	EDE2 A11 ScFv fragment	DENV-2 sE / EDE2 B7 Fab fragment	DENV-2 sE / EDE2 A11 Fab fragment	DENV-2 sE / EDE1 C8 Fab fragment	DENV-2 sE / EDE1 C10 ScFv fragment
PDB ID	4UTC	4UT7	4UT6	4UTB	4UTA	4UT9
Maximum resolution (Å)	**3.1**	**1.7**	**3.2**	**3.85**	**3.0**	**3.2**
Crystallization conditions						
Protein conc. (mg/ml)*	8	1.5	0.7	0.5	0.7	1.5
Crystallization buffer	100mM Tris pH 8.0 86 mM NaFormate 16% PEG 3,350	100mM MES pH 6.5 25% (v/v) PEG MME550 10mM ZnSO4	100mM Tris pH 8.5 16% (w/v) PEG 400 200mM MgCl2	100mM Hepes pH 7.5 10% (w/v) PEG 6,000 5% (v/v) MPD	100mM Tris pH 8.5 18% (w/v) PEG 8,000 200mM Li2SO4	100mM HEPES pH7.5 20% (w/v) PEG 8,000
Cryo-protectant solution	100 mM NaFormate 18% PEG 3,350 15% glycerol 10% PEG 400	No additional cryoprotectant	22% Glycerol in 67% of crystallization solution	Mix of Paratone-N with Paraffin Oil (1:1)	22% Glycerol in 67% of crystallization solution	22% PEG 400 in 67% of crystallization solution
Crystallization method	Hanging drop	Sitting drop	Hanging drop	Sitting drop	Hanging drop	Hanging drop
Data Collection†						
Beamline	ESRF, ID23-2	SOLEIL, PX1	ESRF, ID29	ESRF, ID29	ESRF, ID29	SOLEIL, PX2
Space group	P 4_3 2_1 2	C 2	P 2	P 2_1 2_1 2_1	P 2_1 2_1 2_1	P 1
Unit cell a, b, c (Å)	105.4, 105.4, 165.8	62.9, 47.7, 90.7	101.3, 59, 191.6	58.8, 181.9, 204.8	59.6, 191.3, 203.6	57.5, 102.2, 131.1
α, β, γ (°)	90, 90, 90	90, 102.4, 90	90, 96.2, 90	90, 90, 90	90, 90, 90	91.5, 85.7, 96.1
Resolution (Å)	30-3.1 (3.26-3.1)	30-1.7 (1.73-1.7)	30-3.2 (3.34-3.2)	30-3.85 (4.22-3.85)	30-3.0 (3.11-3.0)	30-3.2 (3.3-3.2)
Measured reflections	301113 (15609)	91989 (2744)	136737 (16536)	102269 (22119)	204824 (20833)	89842 (8410)
Unique reflections	17615 (2395)	28835 (1467)	37500 (4534)	21168 (4997)	45639 (4492)	46477 (4332)
Completeness (%)	99.3 (96.0)	99.3 (95.5)	99.3 (99)	98.3 (98.3)	96.2 (97.6)	95.2 (96.7)
Mn(I) half-set correlation	ND	0.996 (0.811)	0.993 (0.716)	0.981 (0.727)	0.993 (0.560)	0.977 (0.541)
<I / σI>	23.9 (2.5)	8.9 (1.6)	9.2 (1.6)	5.8 (1.4)	7.9 (1.2)	5.0 (1.2)
Rmerge (%)	9.7 (60.9)	7.2 (43.6)	10.9 (64.0)	27.1 (92.5)	12.9 (101.1)	18.7 (55.5)
Structure Determination						
MR search models	1OAN	DENV-2 sE / bnAb EDE2 A11 Fab	DENV-2 sE / bnAb EDE2 A11 Fab	3KDM, 3H0T, 1OKE	3KDM, 3EYF, DENV-2 sE	1OKE
NCS	2	None	2	2	2	4
Targeting	1OAN	None	None	3H0T, 3TJE, DENV-2 sE, bnAb EDE2 A11 ScFv, DENV-2 sE / bnAb EDE2 B7 Fab	3KDM, 3EYF, DENV-2 sE, 1OAN	1OAN
Use of TLS	No	Yes	Yes	No	No	Yes
Refinement‡						
Rcryst. (%) / Rfree (%)	21.1 / 27.9	16.0 / 19.1	21.2 / 25.0	23.0 / 25.7	21.35 / 24.9	20.0 / 24.9
N° of Work/Test reflections	17453 / 882	28441 / 1428	37165 / 1984	21007 / 1070	45462 / 2306	46344 / 2343
N° of protein atoms	6072	2007	9681	12518	12496	19085
N° of heteroatoms	177	214	222	200	252	56
Rms deviation from ideal						
Bond lengths (Å)	0.010	0.010	0.008	0.008	0.010	0.008
Bond angles (°)	1.33	1.03	1.13	1.18	1.28	1.10
Ramachandran plot§						
Favoured (%)	92.1	98.0	91.3	96.1	94.9	91.5
Allowed (%)	6.7	2.0	7.0	3.8	4.8	7.2
Outliers (%)	1.2	0.0	1.7	0.1	0.3	1.3

One crystal was used to collect each of the diffraction data sets used to determined each crystal structure. DENV-2 sE: Den2_FGA-02 (GenBank KM087965). The DENV sE buffer used for all the crystallization experiments was 150 mM NaCl and 15 mM Tris pH 8. Proteins were crystallized at 18 °C.

* Protein concentration was estimated using theoretical extinction coefficients of the complexes (DENV sE + Fab or scFv). Absorbance at 280 nm ($A_{280\,nm}$) of the protein solution was measured before crystallization. The theoretical extinction coefficients for individual component are as follows: DENV-2 sE-His, 1.03; bnAb EDE2 A11 ScFv, 2.08; bnAb EDE2 B7 Fab, 1.65; bnAb EDE2 A11 Fab, 1.68; bnAb EDE1 C8 Fab, 1.52; bnAb EDE1 C10 ScFv, 2.43 (see Methods for more details). Extinction coefficients were calculated without taking into account carbohydrate moieties.

† Highest-resolution shell is shown in parenthesis.

‡ Low resolution for refinements was truncated to 20 Å.

§ Ramachandran statistics were calculated with MolProbity[49].

PEG MME, poly-ethylene glycol monomethyl ether; MPD, 2-methyl-2,4-pentanediol; ND, non-determined; MR, molecular replacement; NCS, non-crystallographic symmetry; TLS, parametrization describing translation, libration and screw-rotation to model anisotropic displacements.

Extended Data Table 2 | Buried surface areas and surface complementarity in the various DENV sE–EDE complexes

	BSA Fab or ScFv			BSA DENV-2 sE					Complex	
	vH	vL	Total	Reference subunit (glycans*)	Opposite subunit (glycans*)	Total (Å^2)	Main chain atoms (Å^2)†	Total glycan BSA (Å^2)	BSA / molecule (Å^2)	SC
DENV-2 sE / EDE2 B7										
Epitope A	992.1	180.8	1172.9	621.1 (83.6)	478.4 (358.0)	1099.5	233 (21.2%)	442 (40%)	1136.2	0.728
Epitope B	1010.4	181.5	1191.9	501.8 (358.0)	604.1 (68.2)	1105.9	234 (21.2%)	426 (39%)	1148.9	0.721
DENV-2 sE / EDE2 A11										
Epitope A	945.1	199.4	1144.5	544.2 (17.80)	491.9 (359.1)	1036.1	224 (21.6%)	377 (36%)	1090.3	0.706
Epitope B	984.8	183.2	1168.0	473.4 (351.4)	587.5 (64.4)	1060.9	221 (20.8%)	416 (39%)	1114.5	0.668
DENV-2 sE / EDE1 C8										
Epitope A	744.2	492.3	1236.5	944.9 (204.9)	234.6	1197.6	362 (30.2%)	204.9 (17%)	1217.1	0.693
Epitope B	855.7	559.2	1414.9	366.4	963.3 (239.2)	1329.4	352 (26.5%)	239.2 (18%)	1372.2	0.687
DENV-2 sE / EDE1 C10‡										
Epitope A	706.6	623.3	1329.9	781.3 (84.5)	366.9	1148.2	351 (31%)	84.5 (7.3%)	1239.1	0.681
Epitope B	706.0	644.4	1350.4	373.2	778.3 (94.20)	1151.5	320 (28%)	94.2 (8.2%)	1251.0	0.681
Epitope C	823.7	562.6	1386.3	717.8 (90.6)	465.6	1183.4	374 (32%)	90.6 (7.6%)	1284.9	0.742
Epitope D	718.1	635.5	1353.6	374.9	788.7 (99.1)	1163.6	341 (29%)	99.1 (8.5%)	1258.6	0.668

BSA, buried surface area (in Å^2) of sE protein by the Fabs or ScFv (calculated with the program 'areaimol' in CCP4); SC, shape complementarity coefficient (calculated with the program 'sc' in CCP4).
* Contribution of glycan chain to buried surface area (in Å^2 and as percentages).
† Contribution of main-chain atoms to buried surface area (in Å^2 and as percentages).
‡ There are two sE dimer-(bnAb C10 ScFv)$_2$ complexes in the asymmetric unit.